



# **East West University**

**Summer -2017**

**Thesis Report**

## **Enhancement of Conversion Efficiency of GaAs/InAs p-i-n Solar Cell Embedding Quantum Dot**

**Submitted by**

Shadman Sakib  
ID: 2013-3-55-005

&

Asma Sadia Prova  
ID: 2013-3-55-015

**Thesis Supervisor**

M. Mofazzal Hossain, Ph.D.  
Professor,  
Department of Electronics and Communications Engineering

## Declaration

We hereby declare that we completed our thesis on the topic entitled “**Enhancement of Conversion Efficiency of GaAs/InAs p-i-n Solar Cell Using Quantum Dot**”. We prepared a thesis report & submitted to follow the terms and condition of the “**Department of Electronic & Communication Engineering**”. This paper is required for fulfillment the degree of B.Sc. in Electronic and Communication Engineering.

We claim that the thesis paper along with its literature which is demonstrated in this report are own work.

.....  
**Shadman Sakib**  
**2013-3-55-005**

&

.....  
**Asma Sadia Prova**  
**2013-3-55-015**

<b>Signature of supervisor:</b>  ----- <b>-Dr.M. Mofazzal Hossain,PhD</b> <b>Professor, Department of Electronics</b> <b>and Communications Engineering,</b> <b>East West University</b> <b>Dhaka, Bangladesh</b>	<b>Signature of chairperson:</b>  ----- <b>--Dr.M.Mofazzal Hossain,PhD</b> <b>Professor, Department of Electronics</b> <b>and Communications Engineering,</b> <b>East West University</b> <b>Dhaka, Bangladesh</b>
--	---

i

## Acknowledgement

First we are grateful to almighty Allah for blessing us to successfully completed the task. A special thanks with honor to our supervisor Dr. M. Mofazzal Hossain for giving us to his valuable time, guidance, motivating thought and encouragement which lead us to success.

We are also pleased to all our faculty member 's of ECE department for their guidance & support to complete our graduation degree. We also thanks to our senior brothers & friends who helps us to make this paper.

A special thanks to our parents whose encouragement and prayer are always with us.

Thank you all for always supporting us.

ii

## **Approval**

This thesis report 'Enhancement of Conversion Efficiency of GaAs/InAs p-i-n Solar Cell Using Quantum Dot.' Submitted by Shadman Sakib ID: 2013-3-55-005 & Asma Sadia Prova ID: 2013-3-55-005, to department of Electronic and Communication Engineering. East West University is submitted in partial fulfillment of the requirement for the degree of B. Sc. In Electronics and Telecommunications Engineering, under complete supervision of the undersigned.

**Approved by:**

-----

Supervisor

Dr.M. Mofazzal Hossain, PhD

Professor,

Department of Electronics and Communication Engineering,

East West University.

iii

## **Abstract**

A high efficiency GaAs/InAs quantum dot (QD) solar cell is designed embedding InAs QD in as an intrinsic layer. Embedded QD boost the efficiency of the solar cell. Without QD we achieve 14.1% efficiency of the GaAs Solar cell. When embedding 15 layers of InAs QDs in the intrinsic layer, at AM1.5 solar radiations, the proposed cell structure had a  $V_{oc}$  of 1.25 V,  $J_{sc}$  of 32.9073 mA.cm<sup>-2</sup>, a maximum power is 36.97mW.cm<sup>-2</sup> and a fill factor of 89.9%, corresponding to an overall efficiency of 36.97%. Therefore, the positive effects of embedded quantum dots are proved to be helpful in improving solar cell's performance.

## Index

### Contents

		<b>Page No.</b>
➤	<b>Chapter 1: Introduction</b>	
	1.1 Solar Energy	1
	1.2 Importance of Solar Energy	2
	1.3 Generation of Solar Energy	3
	1.4 Types of Solar Cell	3
	1.5 Third-generation photovoltaic cell	4
	1.6 What is Quantum Dot	4
	1.7 History of Quantum Dots	5
	1.8 Importance of Quantum Dots	5
	1.9 Physics of Quantum Dots	5
	1.10 Energy Bandgap Vs QD Size	7
	1.11 Energy Band Diagram	8
	1.12 Quantum Dot Solar Cell	8
	1.13 Latest Efficiency Range for QD Cell	8
	1.14 Working Principle of QD Solar Cell	9
	1.15 Purpose of This Thesis	9
➤	<b>Chapter 2: Simulation Methodology</b>	
	2.1 Models	
	2.1.1 Bohm Quantum Potential	10

2.1.2 Fermi	11
2.1.3 Bandgap Narrowing	12
2.1.4 Concentration Dependent SRH	13
2.1.5 Optical Radiative Recombination/Generation	14
2.1.6 Auger Recombination	15
2.1.7 Multiband kp Models	16
2.2 Simulating Photodetectors	
2.2.1 Defining Optical Sources	18
➤ <b>Chapter 3: Simulation &amp; Result</b>	
3.1 Proposed Solar Cell	23
3.2 DQ Solar Cell General Block Diagram	24
3.3 I-V Characteristic Curve Proposed Solar Cell	24
3.2 Simulation of GaAs/InAs QD Solar Cell	25
3.3 Intrinsic Layer	25
➤ <b>Chapter 4: Conclusion</b>	27
➤ <b>Chapter 5: Reference</b>	28

# Chapter 1

## Introduction

### 1.1 Solar Energy

Solar power is the use of the sun's energy either directly as thermal energy (heat) or through the use of photovoltaic cells in solar panels and transparent photovoltaic glass to generate electricity [1]. These two methods are called passive solar energy and active solar energy.

For passive solar energy, concentrated solar power uses multiple lenses or reflectors to collect more of the sun's thermal energy. Thermal energy collected through the day is typically applied to oil or molten salts that retain heat to boil water for steam turbine generators throughout the night [1].

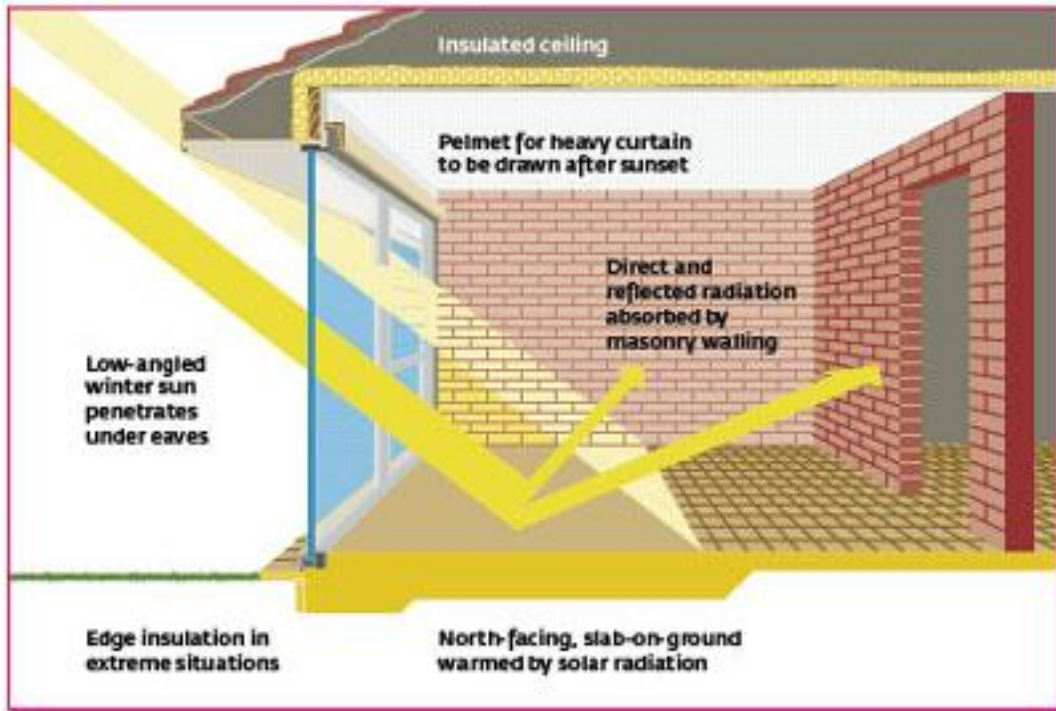


Fig 1: Passive Solar Energy

For active solar energy, a photovoltaic cell (PV cell) is a specialized semiconductor diode that converts visible light into direct current (DC). Some PV cells can also convert infrared (IR) or ultraviolet (UV) radiation into DC electricity. Photovoltaic cells are an integral part of solar-electric energy systems, which are becoming increasingly important as alternative sources of utility power [2].

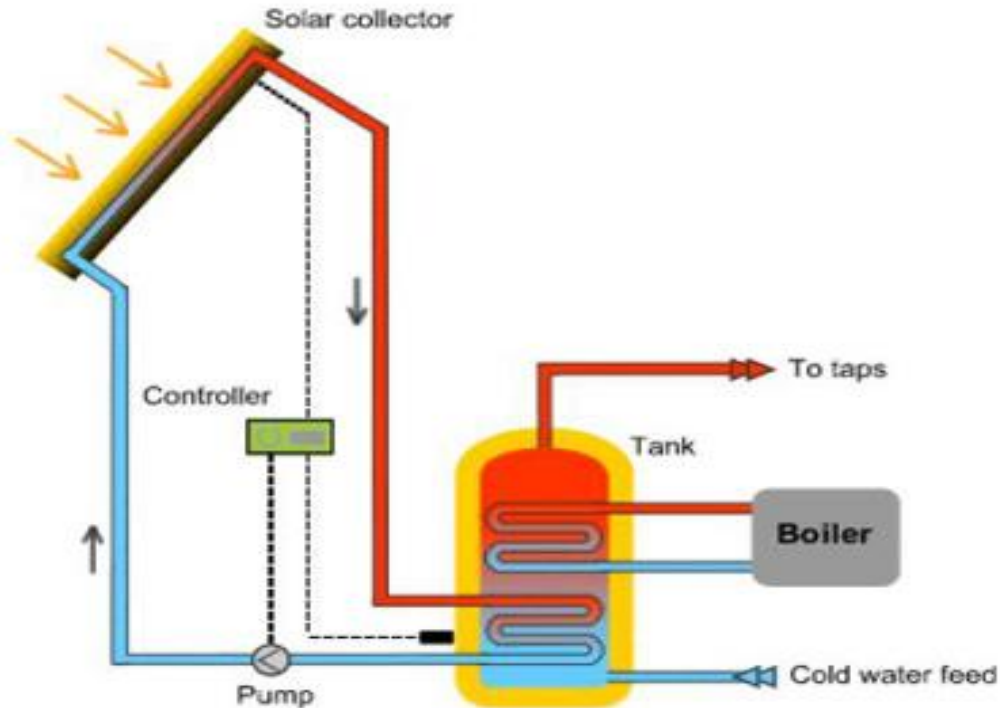


Fig 2: Active Solar Energy

In the data center, solar power and other sources of clean electricity, such as wind power and tidal power, are increasingly implemented to save money, increase self-sufficiency and improve sustainability. Apple, Google and Microsoft are among the major IT companies investing in renewable energy.

Besides being cheaper than fossil fuels, solar power avoids the costs associated with environmental damage through extraction, spills and dealing with pollution created through combustion [1].

## 1.2 Importance of Solar Energy

Solar energy is important because the sun is a sustainable source of energy that can be used to power homes and businesses globally. Fossil fuels are finite and contribute to climate change, so it's important that alternative energy sources be embraced.

Solar energy is a potential solution to the environmental problems being caused by fossil fuels. When fossil fuels are burned to generate electricity, they release harmful greenhouse gases into the atmosphere. Scientists believe that continuing to depend on fossil fuels is going to cause serious environmental problems in the future. Another important use for solar energy is in satellites. Many satellites are engineered with photovoltaic panels, which capture sunlight and convert it into electricity that is used to power the satellite. Solar power is also useful in areas where standard electricity is not available. For example, research facilities in Antarctica depend on sustainable energy sources, such as the sun and wind turbines, to generate power.



Emergency phone systems in remote places use solar power as a dependable power source. Solar energy can also be used to power devices that run at night. For example, some streetlights are able to charge energy from the sun during the day, then run throughout the night [3].

### 1.3 Generation of Solar

The earth receives more energy from the Sun in just one hour than the world's population uses in a whole year. The total solar energy flux intercepted by the earth on any particular day is  $4.2 \times 10^{18}$  Watthours or  $1.5 \times 10^{22}$  Joules (or  $6.26 \times 10^{20}$  Joules per hour). This is equivalent to burning 360 billion tons of oil per day or 15 Billion toe per hour [4]. Moreover, burning these fossil fuels creates carbon dioxide emissions, which are suspected contributor to climate change. In contrast, as long as the sun exists, we can harness its energy here on Earth. And because solar power emits no carbon dioxide, it is an effective solution to natural resource depletion and climate change problems that are becoming more serious every year.

### 1.4 Types of Solar Cell

1. Crystalline Silicon (Monocrystalline & Polycrystalline)
2. Thin-Film Solar Cells (TFSC)
3. Organic Photovoltaic Cell (OPVC)

#### **Crystalline Silicon (Monocrystalline&Polycrystalline)**

This is the first generation silicon based photovoltaic cell. Single crystalline silicon is called monosilicon and the polycrystalline silicon is called polysilicon.

Monocrystalline solar cells are made out of silicon ingots, which are cylindrical in shape. To optimize performance and lower costs of a single monocrystalline solar cell, four sides are cut out of the cylindrical ingots to make silicon wafers, which is what gives monocrystalline solar panels their characteristic look. The efficiency rates of monocrystalline solar panels are typically 15-20%. Monocrystalline silicon solar panels are space-efficient and this kind of solar panels live the longest. But Monocrystalline solar panels are the most expensive and If the solar panel is partially covered with shade, dirt or snow, the entire circuit can break down.

The first solar panels based on polycrystalline silicon, which also is known as polysilicon and multi-crystalline silicon. Unlike monocrystalline-based solar panels, polycrystalline solar panels do not require the Czochralski process. Raw silicon is melted and poured into a square mold, which is cooled and cut into perfectly square wafers. The process used to make polycrystalline silicon is simpler and cost less. Polycrystalline solar panels tend to have slightly lower heat tolerance than monocrystalline solar panels. But the efficiency of polycrystalline-based solar panels is typically 13-16% and lower space-efficiency [5].

## **Thin-Film Solar Cells (TFSC)**

A thin-film solar cell is a second generation solar cell that is made by depositing one or more thin layers, or thin film (TF) of photovoltaic material on a substrate, such as glass, plastic or metal. Thin-film solar cells are commercially used in several technologies, including cadmium telluride (CdTe), copper indium gallium diselenide (CIGS), amorphous thin-film silicon (a-Si, TF-Si). State-of-the-art thin film cells can reach the efficiency of 10-16%, with the highest reported efficiency being 18% [6].

## **Organic Photovoltaic Cell (OPVC)**

An organic solar cell or plastic solar cell is a type of photovoltaic that uses organic electronics, a branch of electronics that deals with conductive organic polymers or small organic molecules, for light absorption and charge transport to produce electricity from sunlight by the photovoltaic effect. Most organic photovoltaic cells are polymer solar cells [7]. Organic solar films developer Heliatek, Dresden, Germany, reports that it has pushed the conversion efficiency of its organic photovoltaic (OPV) cells to 12%, which the company says is equivalent to at least 15% in conventional semiconductor-based cells [8].

### **1.5 Third-generation photovoltaic cell**

Third-generation photovoltaic cells are solar cells that are potentially able to overcome the Shockley–Queisser limit of 31–41% power efficiency for single bandgap solar cells. This includes a range of alternatives to cells made of semiconducting p-n junctions ("first generation") and thin film cells ("second generation"). Common third-generation systems include multi-layer ("tandem") cells made of amorphous silicon or gallium arsenide, while more theoretical developments include frequency conversion, (i.e. changing the frequencies of light that the cell cannot use to light frequencies that the cell can use - thus producing more power), hot-carrier effects and other multiple-carrier ejection techniques.

1. Emerging photovoltaics include:
2. Copper zinc tin sulfide solar cell
3. Dye-sensitized solar cell, also known as "Grätzel cell"
4. Organic solar cell
5. Perovskite solar cell
6. Polymer solar cell
7. Quantum dot solar cell [9].

### **1.6 What is Quantum Dot**

Any material at the nanoscale is a nanoparticle, the material used by nanotechnology researchers to explore new uses for elements in this tiny form. A quantum dot is a nanoparticle made of any semiconductor material such as silicon, cadmium selenide, cadmium sulfide, or indium arsenide.

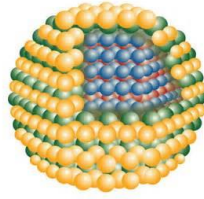


Fig 3: Quantum Dot

## 1.7 History of QD

QDs have been in use since the early 1980's, the expansion of this technology has been hindered as the currently employed synthesis method is very complex, carried out at high temperatures and under an inert atmosphere of argon, time dependent and therefore difficult to control. It does not allow for the process to be easily scaled up. In addition, the current QDs are cadmium based, a toxic element that further limits the use of these dots. Cadmium is banned for use in consumer products in the EU and Japan and an increasing number of countries across the globe are moving to enact similar regulations.

QTG owns the exclusive license with rights to sub-license university based IP that will allow for QDs to be synthesized in an easy, scalable and environmentally friendly manner. This patented synthesis process is carried out at room temperature and normal environmental conditions, is not time dependent and can be run in volumes from milliliters to liter quantities without the need for any significant process modifications. Furthermore, the toxicity will be eliminated by replacing the Cd with non-toxic Zn as the core of the dots. The ability to synthesize non-toxic Zn QDs in large quantities with a consistent quality to allow for these very unique nanoparticles to be applied to a host of technologies ranging from LCDs, LED, solar panels, anti-counterfeiting applications to diagnostics, to name a few [10].

## 1.8 Importance of QD

Companies are exploiting the unique optical effects that occur when semiconductor nanomaterials change size - as the particles are reduced in size, they emit distinctly different colors. The particles can be attached to or incorporated in materials, including biological materials, to act as a kind of barcode or tracking device. One project underway aims to incorporate quantum dots in inks or polymers used in the manufacture of paper money as a way to combat counterfeiting. Currently, quantum dots are used for labeling live biological material in vitro and in vivo in animals (other than humans) for research purposes -they can be injected into cells or attached to proteins in order to track, label or identify specific biomolecules [11].

## 1.9 Physics of quantum dots

In a bulk semiconductor, electrons and holes are free to move and there is no confinement and hence they have continuous energy values, where energy levels are so close to each other and packed such that energy bands are formed. Occupied bands

called valence band and empty ones called conduction bands. The highest occupied band (valence band) and the lowest unoccupied band (conduction band) are separated by what is called energy bandgap  $E_g$ . Exciton is formed when electron hole pair are generated. The bound electron-hole system forms a hydrogen like atom. The separation of between the electron-hole is called Bohr's radius. Table 1 presents examples of exciton Bohr radius for some semiconductors.

Semiconductor Structure	Exciton Bohr Radius (nm)	Bandgap Energy (eV)
PbS	40.0	0.41
GaAs	28.0	1.43
CdTe	15.0	1.50
CdSe	10.6	1.74
ZnSe	8.4	2.58
CdS	5.6	2.53

Table 1. Exciton Bohr radius and bandgap energy of some common semiconductors.

Dimensionality of a material specifies how many dimensions do the carriers of the material act as free carriers. In bulk semiconductor continuous density of states results in both conduction and valence bands. However, when the number of atoms in the lattice is very few, the density of states becomes discrete, and loses the continuous 'band' like feature. Generally speaking, when a material has one or more dimensions small enough to affect its electronic density of state as illustrated in Figure 4, then the material is said to be confined. Accordingly, we can have quantum wells, quantum wires, and quantum dots. Bulk semiconductor materials are example of three dimensional systems where density of states is proportional to  $(E-E_c/v)^{1/2}$ . Quantum well system is a two dimensional system where electrons are confined in one dimension and therefore possess step like density of states. Quantum wire system is a one dimensional system where electrons are confined in two dimensions and therefore possess density of states proportional to  $(E-E_c/v)^{-1/2}$ .

Quantum dot is a zero dimensional system where electron motion is confined in three dimensions. Therefore, a quantum dot possesses atomic like density of states that is described mathematically by a delta function  $\delta(E-E_c/v)$ .

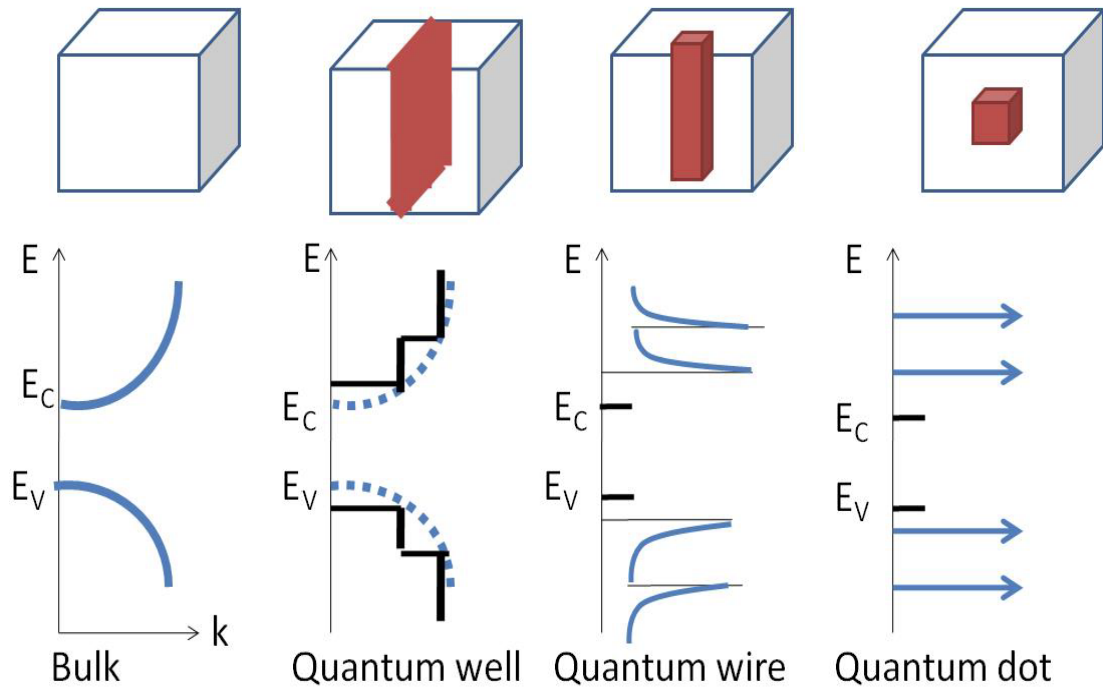


Fig 4: Schematic of density of states as system dimensionality is reduced. The density of states in different confinement configurations: (a) bulk; (b) quantum well; (c) quantum wire; (d) quantum dot. The conduction and valence bands split into overlapping sub bands that become successively narrower as the electron motion is restricted in more dimensions. dimension. Adopted from [13].

### 1.10 Energy Bandgap Vs QD Size

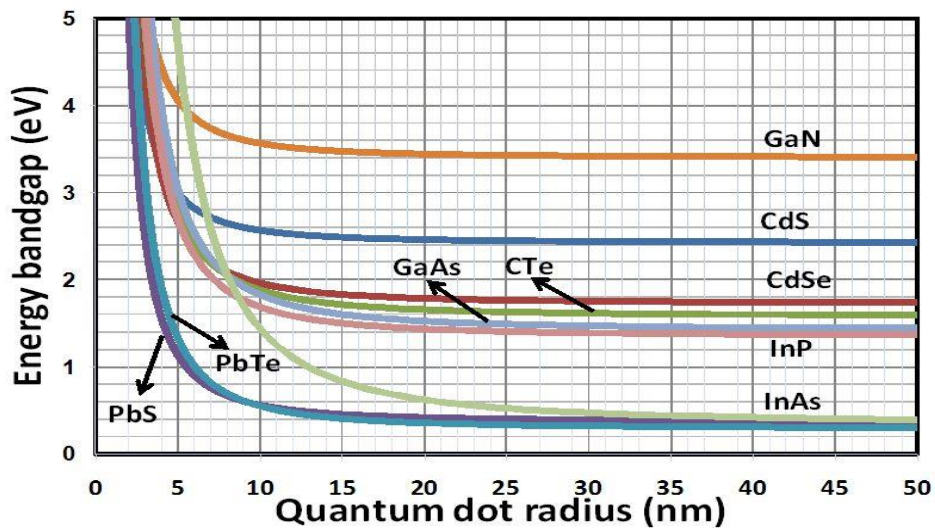


Fig 5: presents few examples of well-known quantum dots, only the first and the second terms have been considered. Other detailed models such as the strong confinement model have been adopted in determining the quantum dot sizes such as CdS [13].

### 1.11 Energy Band Diagram:

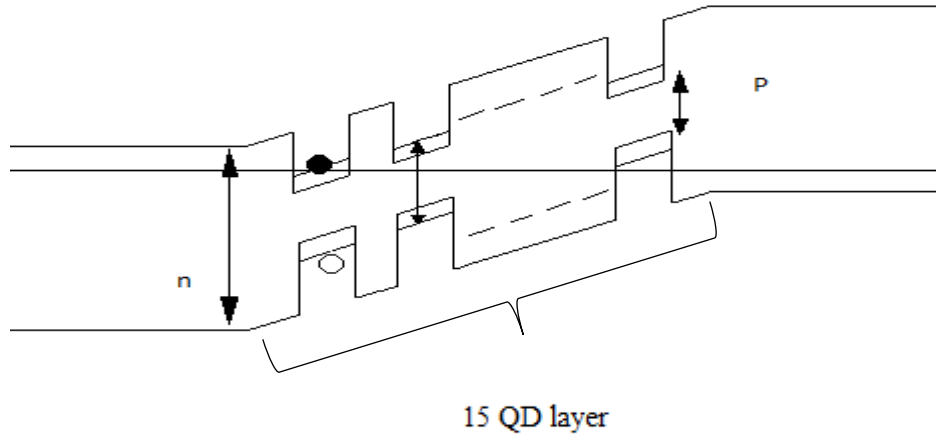


Fig.6: Energy band diagram of the proposed solar cell.

### 1.12 Quantum Dot Solar cell:

A quantum dot solar cell is a solar cell design that uses quantum dots as the absorbing photovoltaic material. It attempts to replace bulk materials such as silicon, copper indium gallium selenide (CIGS) or CdTe. Quantum dots have bandgaps that are tunable across a wide range of energy levels by changing the dots' size. In bulk materials the bandgap is fixed by the choice of material(s). This property makes quantum dots attractive for multi-junction solar cells, where a variety of materials are used to improve efficiency by harvesting multiple portions of the solar spectrum.

### 1.13 Latest Efficiency Range for QD Cell:

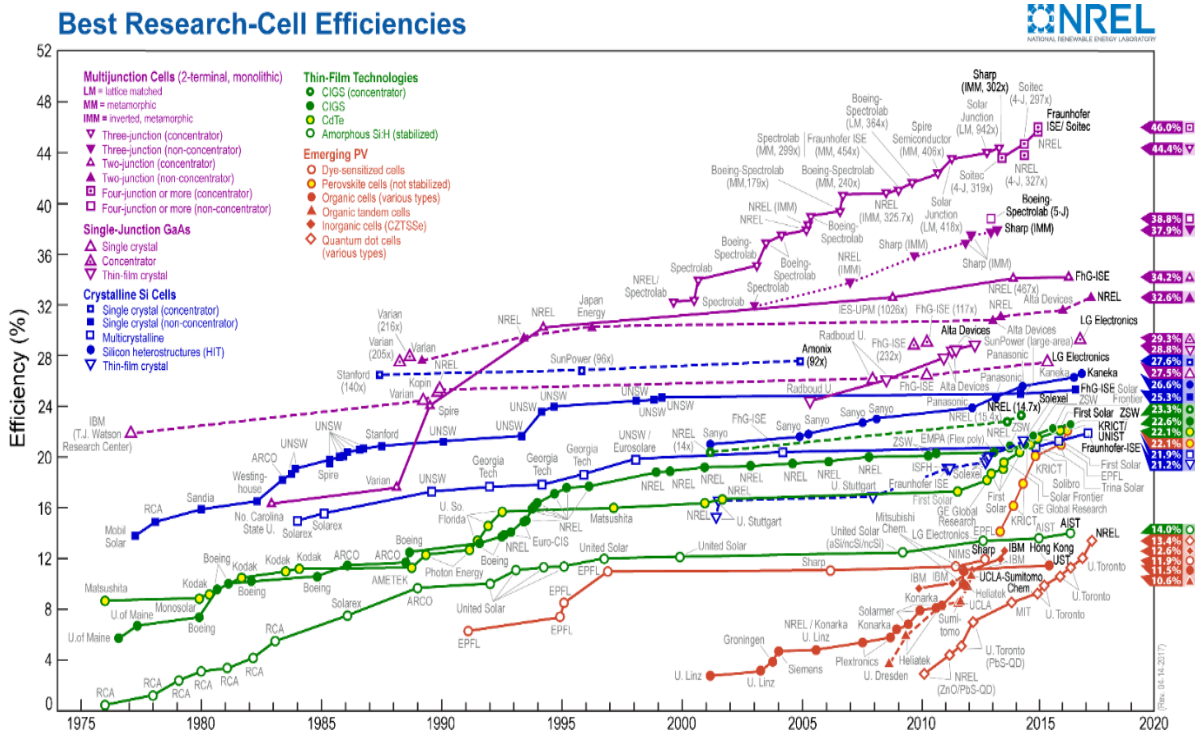


Fig 7: Different Solar Cell Efficiency. Adopted from [14].

### 1.14 Working Principle of QD Solar Cell

Energy levels in quantum dots are quantized due to quantum confinement effect. Tightly arrangement of quantum dots makes the potential barriers narrow, which leads to electrons' co-movement. A sub band is then formed in between conduction band and valence band, which is called intermediate band. Electrons can thus jump from valence band to intermediate band temporarily, and then jump to conduction band with the excitation of another photon, as shown in Fig. 7. Hence, even photons with lower energy than band gap can contribute to photocurrent.

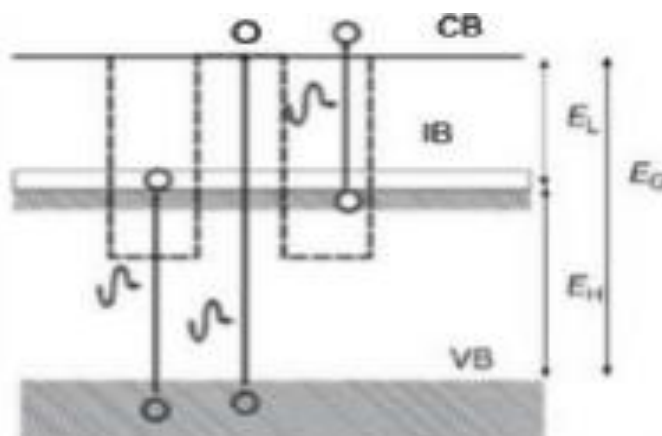


Fig: - 8 Electron transition through intermediate band

In addition, since photons with lower energy have longer wavelength, the absorption range of solar cell can be extended [15].

### 1.15 Purpose of This Thesis

The purpose of this thesis is to design and simulate GaAs/InAsQD solar cell with multiple layer and then compare them to find out the embedded QD's are bring positive effects and improve the performance of solar cell& increasing number of QD layer's gives more efficiency. For this region here we use 2D atlas in SILVACO TCAD software as simulator so the QD are effectively replaced by Quantum Wires.

## Chapter 2

### Simulation Methodology

#### 2.1 Models

In this project for solving QD solar cell we use several methods which are under below,

##### 2.1.1 Bohm Quantum Potential

This model was developed for Silvaco by the University of Pisa and has been implemented into Atlas with the collaboration of the University of Pisa. This is an alternative to the Density Gradient method and can be applied to a similar range of problems. There are two advantages to using Bohm Quantum Potential (BQP) over the density gradient method. First, it has better convergence properties in many situations. Second, you can calibrate it against results from the Schrodinger-Poisson equation under conditions of negligible current flow. The model introduces a position dependent quantum potential,  $Q$ , which is added to the Potential Energy of a given carrier type. This quantum potential is derived using the Bohm interpretation of quantum mechanics and takes the following form

$$Q = \frac{-\hbar^2}{2} \frac{\gamma \nabla(M^{-1} \nabla(n^\alpha))}{n^\alpha} \quad [2.1-2]$$

where  $\gamma$  and  $\alpha$  are two adjustable parameters,  $M^{-1}$  is the inverse effective mass tensor and  $n$  is the electron (or hole) density. This result is similar to the expression for the quantum potential in the density gradient model with  $\alpha = 0.5$ , but there are some differences about how they are implemented.  $Q$  is added to the continuity equations. The Bohm Quantum Potential (BQP) method can also be used for the Energy balance and hydrodynamic models, where the semi-classical potential is modified by the quantum potential the same way as for the continuity equations. The default iterative scheme used to solve the non-linear BQP equation along with a set of semi-classical equations is as follows. After an initial semi-classical solution has been obtained, the BQP equation is solved on its own Gummel iteration to give  $Q$  at every node in the device. The semi-classical potential is modified by the value of  $Q$  at every node and the set of semi-classical equations is then solved to convergence as usual (using a Newton or block iterative scheme). Then, the BQP equation is solved to convergence again and the process is repeated until self-consistency is achieved between the solution of the BQP equation and the set of semi-classical equations. The set of semi-classical equations solved can be any of the combinations usually permitted by Atlas. You can enable an alternative iteration scheme by specifying the BQP.NEWTON flag on the METHOD statement. This causes the BQP equation to be included in the fully coupled Newton iteration. This can only be used with either BQP.N or BQP.P models separately and not with both enabled. Additionally, this model also modifies the intrinsic carrier density,  $n_i$ , by the Bohm quantum potential. This ensures that under equilibrium conditions. On subsequent SOLVE statements, the FREEZEBQPNI flag should be enabled to ensure that the value of  $n_i$  used is the equilibrium one to use the BQP model for electrons (or holes), specify BQP.N (BQP.P) in the MODELS



statement. You can also set the parameter values ( $\gamma$  and  $\alpha$ ) and the direction of the quantization (confinement).

Tables 2.1 and 2.2 show the parameters to use for the MODELS statement.

**Table 2.1 MODEL Statement Parameters for Electrons**

Parameter	Type	Default	Units
<b>BQP.N</b>	Logical	false	
<b>BQP.NGAMMA</b>	Real	1.2	--
<b>BQP.NALPHA</b>	Real	0.5	--
<b>BQP.QDIR</b>	Integer	2	--

**Table 2.2 MODEL Statement Parameters for Holes**

Parameter	Type	Default	Units
<b>BQP.P</b>	Logical	false	
<b>BQP.PGAMMA</b>	Real	1	--
<b>BQP.PALPHA</b>	Real	0.5	--
<b>BQP.QDIR</b>	Integer	2	--

### 2.1.2 Fermi

Fermi-Dirac reduced carrier concentrations in heavily doped regions. Electrons in thermal equilibrium at temperature TL with a semiconductor lattice obey Fermi-Dirac statistics. That is the probability  $f(\epsilon)$  that an available electron state with energy  $\epsilon$  is occupied by an electron is:

$$f(\epsilon) = \frac{1}{1 + \exp\left(\frac{\epsilon - E_F}{kT_L}\right)} \quad [2.3]$$

Where,

$E_F$  = A spatially independent reference energy known as the Fermi level

$k$  = is Boltzmann's constant.

If  $\epsilon - E_F \gg kT_L$ , then the above equation can be express as,

$$f(\epsilon) = \exp\left(\frac{\epsilon - E_F}{kT_L}\right) \quad [2.4]$$

### 2.1.3 Bandgap Narrowing

In the presence of heavy doping, greater than  $10^{18} \text{cm}^{-3}$ , experimental work has shown that the pn product in silicon becomes doping dependent. As the doping level increases, a decrease in the bandgap separation occurs, where the conduction band is lowered by approximately the same amount as the valence band is raised. In ATLAS this is simulated by a spatially varying intrinsic concentration  $n_i$  defined according to equation

$$n_{ie}^2 = n_i^2 \exp\left(\frac{\Delta E_g}{kT}\right) \quad [2.5]$$

Bandgap narrowing effects in ATLAS are enabled by specifying the BGN parameter of the MODELS statement. These effects may be described by an analytic expression relating to the variation in bandgap,  $\Delta E_g$ , to the doping concentration,  $N$ . The expression used in ATLAS is from Slotboom and de Graaf:

$$\Delta E_g = BGN.E \left\{ \ln \frac{N}{BEG.N} + \left[ \left( \ln \frac{N}{BGN.N} \right)^2 + BGN.C \right]^{\frac{1}{2}} \right\} \quad [2.6]$$

We can specify the BGN.E, BGN.N, and BGN.C parameters in the MATERIAL statement. The default values from Slotboom and Klaassen are shown in Table 2.3. The Klaassen defaults will be used if you specify the BGN.KLA parameter in the MODELS statement. Otherwise, the Slotboom values will be used (by default). You can select a second set of defaults by specifying BGN.KLASSEN.

**Table 2.3 Parameters for Bandgap Narrowing Model**

Statement	Parameter	Values	Unit
MATERIAL	BGN.E	0.009	eV
MATERIAL	BGN.N	$1 \times 10^{17}$	$\text{cm}^{-3}$
MATERIAL	BGN.C	0.5	-

### 2.1.4 Concentration Dependent SRH

Phonon transitions occur in the presence of a trap within the forbidden gap of the semiconductor. This is essentially a two-step process, the theory of which was first derived by Shockley and then by Hall. The Shockley-Read-Hall recombination is modeled as follows:

$$R_{SRH} = \frac{pn - n_{ie}^2}{TAUPO \left[ n + n_{ie} \exp\left(\frac{ETRAP}{kT_L}\right) \right] + TAUNO \left[ p + n_{ie} \exp\left(\frac{-ETRAP}{kT_L}\right) \right]} \quad [2.7]$$

Where,

ETRAP = The difference between the trap energy level and the intrinsic Fermi level

TL = The lattice temperature in degrees Kelvin

TAUNO = The electron lifetimes

TAUPO = The hole lifetimes.

This model is activated by using the SRH parameter of the MODELS statement. The electron and hole lifetime parameters, TAUNO and TAUPO, are user-definable in the MATERIAL statement. The default values for carrier lifetimes are shown in Table 2.1. Materials other than silicon will have different defaults.

**Table 2.4 Parameters**

Statement	Parameter	Default	Units
MATERIAL	ETRAP	0	eV
MATERIAL	TAUNO	$1 \times 10^{-7}$	s
MATERIAL	TAUPO	$1 \times 10^{-7}$	s

The constant carrier lifetimes that are used in the SRH recombination model above can be made a function of impurity concentration using the following equation:

$$R_{SRH} = \frac{pn - n_{ie}^2}{\tau_p \left[ n + n_{ie} \exp\left(\frac{ETRAP}{kT_L}\right) \right] + \tau_n \left[ p + n_{ie} \exp\left(\frac{-ETRAP}{kT_L}\right) \right]} \quad [2.8]$$

Where,

$$\tau_n = \frac{TAUNO}{AN + BN \left( \frac{N_{total}}{NSRHN} \right) + CN \left( \frac{N_{total}}{NSRHN} \right)^{EN}}$$

$$\tau_p = \frac{TAUPO}{AP + BP \left( \frac{N_{total}}{NSRHP} \right) + CP \left( \frac{N_{total}}{NSRHP} \right)^{EP}}$$

Here,

$N$  = The local impurity concentration.

The TAUN0, TAUP0, NSRHN, and NSRHP parameters can be defined on the MATERIAL statement. This model is activated with the CONSRH parameter of the MODELS statement.

**Table 2.5 Parameters**

Statement	Parameter	Default	Units
MATERIAL	TAUN0	1	s
MATERIAL	NSRHN	$-1 \times 10^3$	cm <sup>-3</sup>
MATERIAL	TAUP0	1	s
MATERIAL	NSRHP	$-1 \times 10^3$	cm <sup>-3</sup>
MATERIAL	AN	1	
MATERIAL	AP	1	
MATERIAL	BN	0	
MATERIAL	BP	1	
MATERIAL	CN	0	
MATERIAL	CP	0	
MATERIAL	EN	0	
MATERIAL	EP	0	

### 2.1.5 Optical Radiative Recombination/Generation

OPTR selects the optical recombination model. When this parameter is specified, the COPT parameter of the MATERIAL statement should be specified. The next physical mechanisms we have to consider for generation/recombination are photon transition. This mechanism occurs primarily in one step and is therefore a direct generation/recombination mechanism. There are two partial processes involved. For radiative recombination, an electron loses energy on the order of the band gap and moves from the conduction band to the valence band. For optical generation, an electron moves from the valence band to the conduction. In silicon, band to band generation/recombination is insignificant. This effect, however, is important for narrow gap semiconductors and semiconductors whose specific band structure allows direct transitions. By assuming a capture rate  $C_{COPT}$  and an emission rate  $C_{EOTP}$ ,

The involved partial processes can be written as,

$$R_{np}^{OPT} = C_c^{OPT} n_p \quad [2.9]$$

for recombination and

$$G_{np}^{OPT} = C_e^{OPT} \quad [2.10]$$

for generation

These rates must be equal in thermal equilibrium so that

$$C_{np}^{OPT} = C_c^{OPT} n_{ie}^2 \quad [2.11]$$

The total band to band generation/recombination is the difference of the partial rates, which equates to

$$R_{np}^{OPT} = C_c^{OPT} (np - n_{ie}^2) \quad [2.12]$$

In ATLAS, COPT is used express CcOPT and can be defined away from default values on the materials statement or implemented using a C-Interpreter routine. To turn on the optical recombination/ generation model, define the OPTR keyword on the MODELS statement.

### 2.1.6 Auger Recombination

Auger is the Direct Recombination Model. Auger recombination occurs through a three particle transition whereby a mobile carrier is either captured or emitted. It is important at high current densities. The underlying physics for such processes is unclear and normally a more qualitative understanding is sufficient. Auger Recombination is commonly modeled using the expression:

$$R_{AUGER} = AUGN (pn^2 - nn_{ie}^2) + AUGP (np^2 - pn_{ie}^2) \quad [2.13]$$

Where the model parameters AUGN and AUGP are user-definable in the MATERIAL statement. We can activate this model with the AUGER parameter from the MODELS statement.

**Table2.4 Parameters for Equation**

Statement	Parameter	Value	Units
MATERIAL	AUGN	0	cm6/s
MATERIAL	AUGP	0	cm6/s

U. AUGER specifies that the integrated Auger recombination rate is to be extracted.

### 2.1.7 Multiband kp Models

The spatially dependent k.p model is automatically enabled for each region associated with a MODELS statement. We name such a region a “quantum region” for sake of clarity below. By default, each quantum region is treated independently from the rest with the Dirichlet boundary condition of vanishing wave functions at its boundary. Coupled models are generated by default by specifying QWELL or SLATT. When using the k.p models, SLATT and QWELL are equivalent and below we only refer to QWELL.

If the QWELL parameter is true for any quantum region, then that region is combined with the quantum regions that are its neighbors in real space. If the k.p models for the two regions are different sub-models of the 8-band model, then a larger model containing the basis states of both is defined for the combined region.

The above process continues until each quantum region with QWELL is surrounded by regions. Therefore, the presence of QWELL flag results in treating all neighboring quantum regions as coupled by default, which yields the coupled multiple quantum well model. The other important aspect of this flag is to perform the calculation of linear optical response for the full quantum region automatically after solving for the band structure. However, Atlas keeps track of the sub-regions for which you have specified the QWELL parameter on the REGION or MODELS statements. It localizes the computed optical response to those sub-regions, scaling the gain coefficient by the ratio L/R, where L is the full length of the quantum region, and R is the sum of the lengths of the sub-regions for which QWELL is explicitly specified. This allows multiple quantum wells to be treated as coupled. Only one expensive calculation is then performed per corrector cycle. At the same time, the optical gain is localized to the well region for use in the drift-diffusion and photon rate equations.

In systems confined in one spatial direction, the optical gain (absorption) coefficients are dimensionless. They represent the fraction of photons generated (absorbed) from a flux incident on the quantum region. However, it is common practice to maintain the uniformity of definitions and divide the optical gain in 2D systems by the length of the confinement direction. Furthermore, along the confinement direction, we can only determine the wave function and associated probabilities of locating a carrier. This prevents specification of gain and radiative recombination localized to a point in space, as required in drift diffusion and photon rate equations. Using QWELL parameter as described above allows you to localize the gain to a small but finite volume. This type of locality is necessary to interface the model with the classically motivated rate equations. In certain cases, especially if the amalgamated region becomes too large, this classical locality with the quantum mechanical results can be made more consistent by preventing one or more regions to be joined with others. This allows you full control over the extent to which the quantum region expands automatically.

You can exclude a particular region completely from the procedure joining multiple regions. In this case, specify a different value for the QWNUM parameter at the REGION statement. Regions are combined as above only if they have the same QWNUM value. They must also have the same confinement direction specified by the SP.GEOM parameter. An alternative route to achieving the same effect is to define

disjoint quantum regions, so that two regions marked for quantum calculation via the parameters in Table 2.1 are separated by a region for which none of the parameters are true.

A separate calculation is performed for each independent quantum region. The quantum regions (after expansion) are then allowed to overlap. This results in multiple values of physical quantities at mesh nodes lying within the overlap of quantum regions. In this case, the average of the multiple values will be computed at those nodes.

Once a set of quantum regions is identified as described above, a 1D spatial mesh is applied across each region along the orientation defined by the SP.GEOM parameter. The orientation is currently assumed to be the [001] crystallographic direction. The grid spacing is set to the average grid spacing of the Atlas mesh inside the region. This can be overridden for one or more regions by specifying the WELL.NY (for 1DY) or WELL.NX (for 1DX) on the MODELS statement for the corresponding regions. The mesh is duplicated to create a uniform distribution of slices along the direction orthogonal to the orientation. The number of slices is set by WELL.NX (for 1DY) or WELL.NY (for 1DX) if specified. Otherwise, this number is also determined by setting the spacing between the slices to be the average grid spacing of Atlas mesh in the corresponding direction.

Atlas solves the Schrodinger equations of a k.p model using the method of finite elements. By default, second order polynomials are used in each cell of the spatial mesh. The cell basis are converted to nodal basis via the wave function continuity imposed at each cell boundary. The default corresponds to the KP.FEM.LAGRANGE parameter on the MODELS statement, which uses second order polynomials. The order can be changed to third order Hermite polynomials by specifying KP.FEM.HERMITE. With Hermite polynomials, the extra degree of freedom can be used to match the derivatives of the wave functions by integrating the matrix k.p equation across each cell boundary. This results in a scattering matrix relating the coefficients in one cell to its neighbors, and yields the same number (but different type) of nodal basis as in the second order case. To activate matching, specify KP.FEM.INTERFACE on the MODELS statement. A different scattering matrix must be constructed at each k when derivative matching is on. This results in different nodal bases (and a different overlap matrix) at each k, which is more time consuming than the second order case. You can quantify corrections arising from explicit derivative matching for a particular problem by comparing results with KP.FEM.INTERFACE set to True with those when KP.FEM.INTERFACE is set to False.

## 2.2 Simulating Photodetectors

This section describes techniques to simulate photodetectors. This section applies to the simulation of the following devices: p-n and p-i-n photodiodes, avalanche photodiodes, Schottky photodetectors, CCDs, MSMs, photoconductors, optical FETs and optically triggered power devices.

As a consequence of the periodicity of the crystal potential, the general form of the single electron eigenstates of the crystal is guaranteed by the Bloch theorem to be

### 2.2.1 Defining Optical Sources

We can define up to ten optical sources. Optical sources are described by using the BEAM statement. All BEAM statements must appear somewhere after the MESH, REGION, DOPING, and ELECTRODE statements and before any SOLVE statement. The parameters in the BEAM statement describe a single optical source.

The NUM parameter is used to uniquely identify one optical source. Values between 1 and 10 are valid for the NUM parameter. Optical sources are subsequently referred to by the value of their NUM parameter. The power of the optical beam is set by using the B<n> parameter of the SOLVE statement, where n is the beam number defined by NUM.

The ANGLE parameter specifies the angle of the direction of propagation of the beam with respect to the device coordinate system. ANGLE=90 specifies vertical (normal) illumination from above. The optical source can be either monochromatic or multispectral. For monochromatic sources, we can use the WAVELENGTH parameter to assign the optical wavelength. WAVELENGTH uses the unit microns to be more consistent with the rest of ATLAS. For multispectral sources, spectral intensity is described in an external ASCII file indicated by the POWER.FILE parameter. This is a text file that contains a list of pairs defining wavelength and spectral intensity. The first line of the file gives the integer number of wavelength-intensity pairs in the file. An example of such a file is shown below.

```
4
0.4 0.5
0.5 1.0
13

0.6 1.2
0.7 1.1
```

This example specifies that there are four samples and that at a wavelength of 0.4  $\mu\text{m}$ , the intensity is 0.5 Watts per square cm per  $\mu\text{m}$  of wavelength, and so on. With multispectral sources, specify a discretization of the interpolated information. Values must be specified for the WAVEL.START, WAVEL.END, and WAVEL.NUM parameters. These values specify the starting and ending wavelengths and the number of wavelengths to sample. LUMINOUS uses wavelengths at equal intervals over a specified range of wavelengths.

If we don't specify the values of WAVEL.START, WAVEL.END, and WAVEL.NUM, these parameters take on the corresponding values from the specified POWER.FILE. For the example file shown above, LUMINOUS uses the following default values of these parameters:

WAVEL.START=0.4, WAVEL.END=0.7, and WAVEL.NUM=4.

LUMINOUS performs an independent ray trace at each of the sample wavelengths.

For example:

WAVEL.START=0.4 WAVEL.END=0.6 WAVEL.NUM=2



causes ray traces at wavelengths of 0.45 and 0.55. LUMINOUS obtains the intensity associated with each sample by integrating the values of the spectral intensity file using a piece wise linear approximation. Each integral is performed over the range between successive midpoints. In the preceding example, the integration for the sample at 0.45 would be performed over the range of 0.4 to 0.5.

For a multispectral source, the generation rate is given by:

$$G = \eta_0 \int_{WAVEL.START}^{WAVEL.END} \frac{P(\lambda)L\lambda}{hc} \alpha e^{-\alpha y} d\lambda \quad [2.14]$$

Where,

$\eta_0$  = The internal quantum efficiency.

$P(\lambda)$  = The power spectral density of the source.

$L$  = A factor representing the cumulative loss due to reflections, transmissions, and absorption over the ray path.

$\lambda$  = The wavelength.

$h$  = Planck's constant.

$c$  = The speed of light.

$\alpha$  = The absorption coefficient

$y$  = The depth of the device, where  $x, y$  forms the two-dimensional mesh.

$WAVEL.START$  = The starting of spectral limits specified on the BEAM statement

$WAVEL.END$  = The ending of spectral limits specified on the BEAM statement.

The source photocurrent is given by:

$$IS = qBn h c W \int (\lambda) d\lambda WAVEL.END WAVEL.START$$

Where,

$P(\lambda)$  = The power spectral density of the source.

The other parameters have the same definition as in Equation

The available photo current is given by:

$$IA = qBn h c$$

$$\sum W r N r i = 1 \int \int (\lambda) WAVEL.END WAVEL.START X i 0 \alpha i e^{-\alpha i Y} P i dy d\lambda \quad [2.15]$$

where

$P(\lambda)$  = The power spectral density of the source.

The other parameters have the same definition as in Equation.

LUMINOUS allows you to choose the units of spectral intensity in an input spectrum file. By default, the units of spectral intensity in the POWER.FILE are W/cm<sup>2</sup>. In this case, LUMINOUS carries out the integration. If the units of spectral intensity in the POWER.FILE are W/cm<sup>2</sup>, then you need to use the flag INTEGRATE

on the BEAM statement. In this case, each value  $P(\lambda)$  in the second column of the file is a total intensity for a corresponding spectral interval. Integrals over spectrum are reduced to summations of  $P(\lambda)$  values. In both cases, LUMINOUS treats the subsequently specified value of  $B_n$  on the SOLVE statement as a unit less multiplier or scale factor for intensity.

This is different from monochromatic case where this parameter has units of  $W/cm^2$ . To preserve consistency with monochromatic case, you can also do the same in the multispectral applications. If you specify the total beam intensity for multispectral sources using  $B_n$  parameter

on the SOLVE statement, you need to set NORMALIZE flag on the BEAM statements. This ensures that the intensity spectrum is normalized and  $B_n$  has units of  $W/cm^2$ .

One of the simpler tasks in characterizing a photodetector design is to measure DC detection efficiency. This will be done typically as a function of bias voltage, optical intensity, or wavelength. Each of these analyses can be performed using the SOLVE statement. The  $B_n$  parameter can be used to set the optical intensity of the optical sources described in the previous section. The following example illustrates obtaining a solution with a specified optical intensity:

```
SOLVE B1=1.0
```

This specifies that a solution is to be obtained for an optical intensity in the beam numbered "1" of  $1.0 \text{ Watt/cm}^2$ . If this were the first SOLVE statement specified, the ray trace in LUMINOUS would be initiated. At the start of the solution, the optical intensities of each optical source with a positive intensity is printed. In addition, the available photocurrent and source photocurrent are printed.

The available photocurrent divided by the source photocurrent is a measure of the external quantum efficiency of the detector. The calculated terminal current can be divided by the source or available photocurrents is used to evaluate the internal quantum efficiency of the device. To obtain VOC and ISC for a solar cell, first define the illumination conditions. This should be done as discussed above in describing multi-spectral sources. The short circuit current is obtained by defining the contacts as voltage dependent contacts (default) and obtaining a solution with the device under zero bias with illumination. This can typically be done as a first step by the following input statement, for example:

```
SOLVE B1=1
```

In this statement, it's assumed the source,  $B_1$ , has been already defined and the intensity is expected in the actual device. When you obtain a solution, the terminal currents represent the short circuit current. The open circuit voltage is obtained by defining one or more of the contacts as current controlled. This is done using the CONTACT statement. For example:

```
CONTACT NAME=anode CURRENT defines that electrode number 1 is a current controlled electrode.
```

The response of photodetectors to angle of incidence can be obtained in a manner analogous to the method used to obtain spectral response. In this case, the ANGLE parameter of the SOLVE statement specifies an angle added to the value of the BEAM parameter PHI (ANGLE). This allows collection of response versus angle. The following examples statements demonstrate the syntax.

```
SOLVE B1=1 ANGLE=0
SOLVE B1=1 ANGLE=10
SOLVE B1=1 ANGLE=20
SOLVE B1=1 ANGLE=30
SOLVE B1=1 ANGLE=40
SOLVE B1=1 ANGLE=50
SOLVE B1=1 ANGLE=60
```

Equivalently, you may find it more convenient to specify an angle ramp. To specify a ramp of angle, you should assign the BEAM parameter to the beam index of the optical source to be ramped. Also, you should specify the initial angle with the ANGLE parameter, the final angle with the AFINAL parameter, and the angle step size with the ASTEP parameter as illustrated in the following.

```
SOLVE B1=1 BEAM=1 ANGLE=0.0 ASTEP=10.0 AFINAL=60.0
```

This is completely analogous to the seven statements described above.

Luminous 2D provide flexible means for defining multispectral sources. In addition, you can directly access built-in public domain solar spectra for am0 and am1.5 conditions by specifying AM0 or AM1.5 on the BEAM statement. These spectra consist of numerous samples.

The following is an example of how you might define the BEAM statement for analysis of am1.5 conditions with subsampling.

```
BEAM NUM=1 AM1.5 WAVEL.START=0.3 WAVEL.END=1.0
WAVEL.NUM=50
```

Here, we are choosing to simulate am1.5 conditions sampled between 0.3 microns and 1.0 microns at 50 samples. We do not have to worry about sampling the many peaks and valleys in the solar spectrum as it is automatically integrated into each subsample. The subsampling effects only the number of wavelengths for which the propagation model is calculated not the integrated intensity. Ray tracing is the principal propagation model for cases where we are not concerned about interference or diffraction effects in the bulk of the device. This is most useful for relatively thick bulk devices, such as crystalline silicon devices. It is useful for planar or textured devices.

For textured devices, the texturing must be described explicitly in the device structure. The following gives an example of the specification of ray tracing for the optical propagation model for Luminous.

BEAM NUM=1 AM1.5 WAVEL.START=0.3 WAVEL.END=1.0  
WAVEL.NUM=50

In this case, we will perform 50 ray traces. The omission of other model keywords, such as TR. MATRIX, FDTD, or BPM, signifies that ray tracing will be performed.

For Luminous, the algorithm automatically traces exactly the right number of rays to completely resolve all discontinuities at the surface and deep into the device. Here, we will describe how to extract the most common figures of merit for solar cells. These extraction methods are solution strategies placed in your input deck after defining the device structure, physical models, and the optical source as described in the previous section.

Typically, the first step in solar analysis is to illuminate the device. You can turn on the illumination by assigning the beam intensity on a SOLVE statement as follows:

```
SOLVE B1=1.0
```

Here, we assign a value of one "sun" to the intensity of the optical source indexed as number "1" (B1).

As we had assigned AM1.5 on the BEAM statement, this corresponds to standard test conditions. In some cases, we may encounter convergence difficulties and may need to ramp the light intensity as shown in the following:

```
SOLVE B1=1.0
```

You may also choose to assign the beam intensity to a value greater than one to simulate solar concentrator effects. Since we have not yet assigned any bias voltages, the current in the run time output corresponds to the short circuit current (Isc).

# Chapter 3

## Simulation & Result

### 3.1 Proposed Solar Cell

After designing and simulation of QD Solar Cell in SILVACO the proposed solar cell under below,

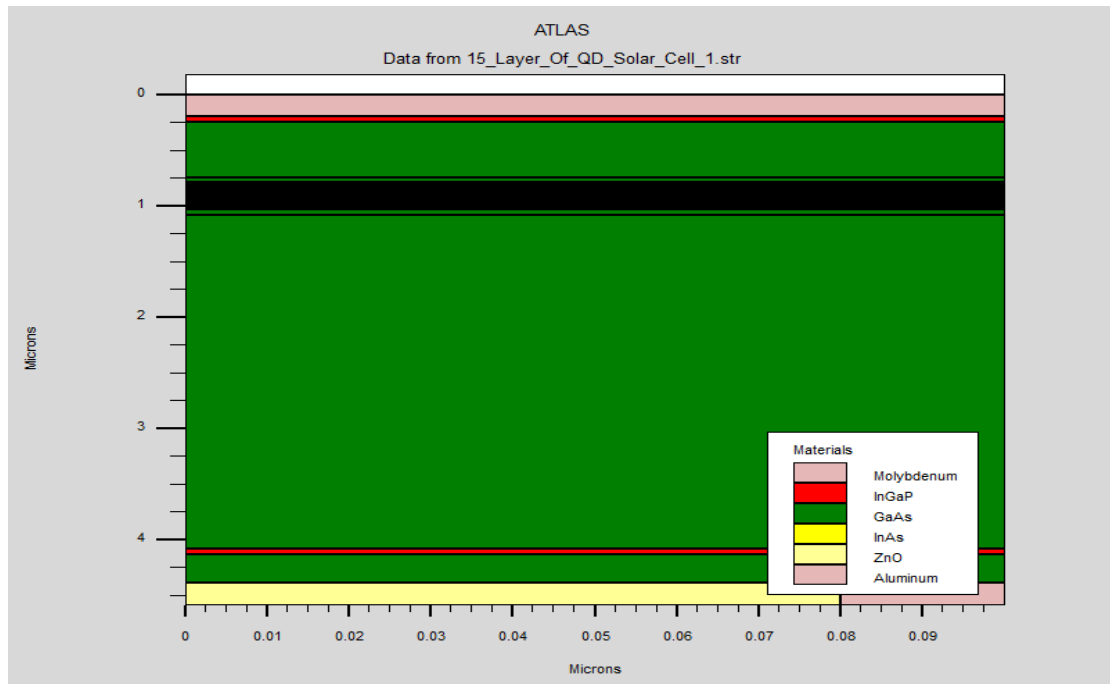


Fig: 3.1 Structure of GaAs/InAs QD Solar cell

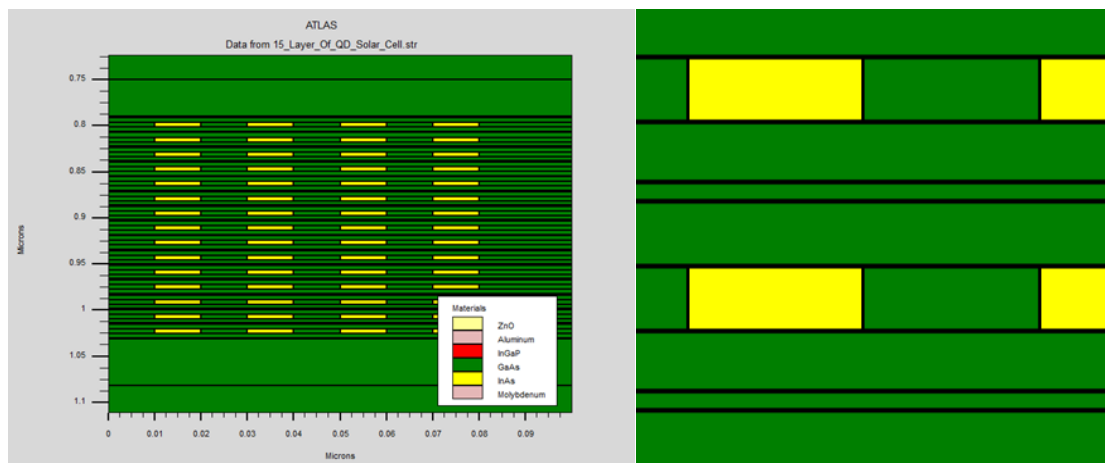


Fig: 3.2 Zoomed-in view of 15 layers' quantum dots inserted in intrinsic region

### 3.2 General Block Diagram proposed QD Solar Cell

This is the general block diagram of proposed QD solar cell where the thickness of the cell at y axis is  $4.67\mu\text{m}$  and at x axis is  $.1\mu\text{m}$ .

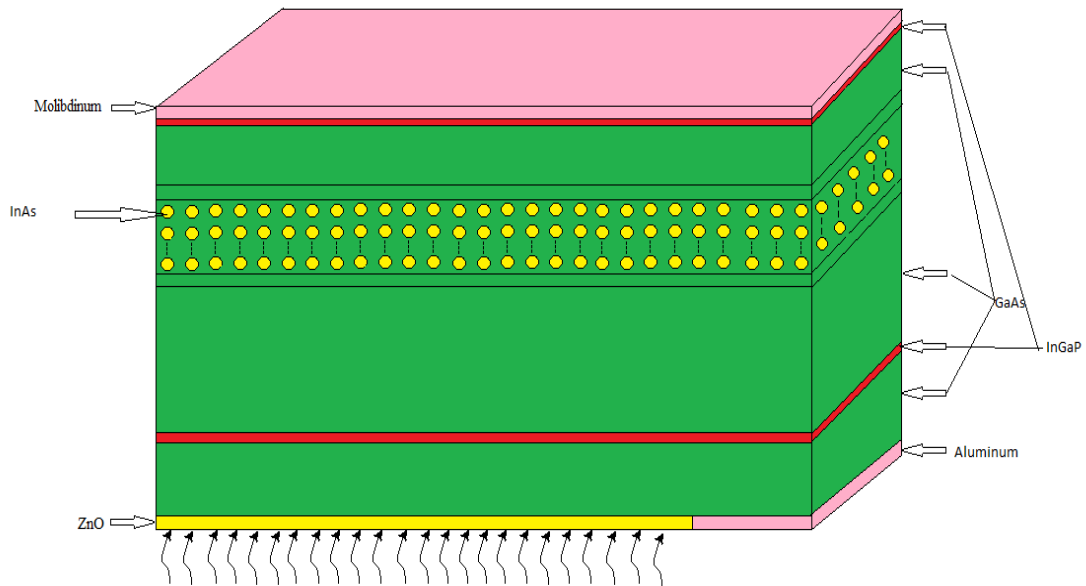


Fig 3.3: General Block Diagram of QD Solar Cell

### 3.3 I-V Characteristic of proposed cell

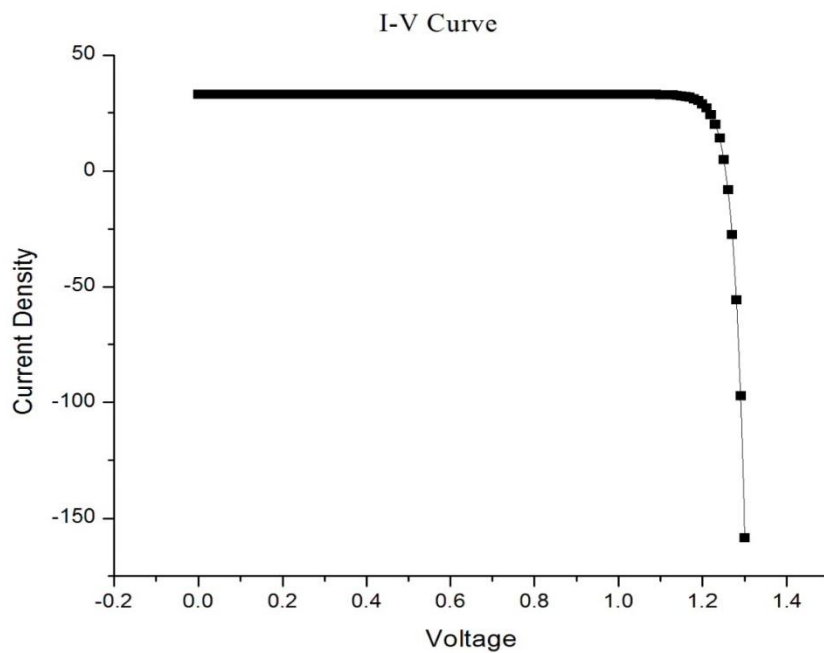


Fig 3.4: Proposed Solar Cell IV Characteristic Curve

### 3.4 Simulation of GaAs/InAs QD Solar Cell

In simulation of GaAs/InAs QD solar cell QD are embedded in intrinsic layer and top of the intrinsic layer we use n-type InGaP and GaAs layer and at the bottom of the intrinsic layer we use same material as a p-type. At the front we use Aluminum and bottom we use Molibdinum as a front and back contact. The QD's that are used in the intrinsic layer are replaced by quantum Wire. For the increasing no of quantum dot layers, we get different efficiency are given below,

Table- 3.1: Efficiency for Different Layer

Device	$J_{sc}(mA/cm^2)$	$V_{oc}(volts.)$	Fill factor (%)	Efficiency (%)
5-layers QDs	32.06	1.24	89.6	35.60
10-layers QDs	32.51	1.24	89.7	36.30
15-layers QDs	32.90	1.25	89.9	36.97

From this table, if we increase the number the of QD layer the short circuit current, open circuit voltage, fill factor and efficiency are also increased that means if we embedded more quantum dot layer in the intrinsic layer we can boost up the efficiency.

Table 3.2: Intrinsic layer properties for 1 layer

Name	Material	Width( $\mu m$ )	Height(nm)
Barrier	GaAs	.10	1.5
Barrier	GaAs	.10	5
Well	InAs	.01	5
Barrier	GaAs	.10	4.5

This is for only one QD layer which are embedded in intrinsic layer.

### 3.5 Intrinsic Layer

PIN photodiodes are used in fiber optic network cards and switches. As a photo detector, the PIN diode is reverse biased. Under reverse bias, the diode ordinarily does not conduct (save a small dark current or leakage). When a photon of sufficient energy enters the depletion region of the diode, it creates an electron-hole pair. The reverse bias field sweeps the carriers out of the region creating a current. Some detectors can use avalanche multiplication.

The same mechanism applies to the PIN structure, or p-i-n junction, of a solar cell. In this case, the advantage of using a PIN structure over conventional semiconductor p-n junction is the better long wavelength response of the former. In case of long wavelength irradiation, photons penetrate deep into the cell. But only those electron-hole pairs generated in and near the depletion region contribute to current generation. The depletion region of a PIN structure extends across the intrinsic

region, deep into the device. This wider depletion width enables electron-hole pair generation deep within the device. This increases the quantum efficiency of the cell.



## **Chapter 4**

### **Conclusion**

In this thesis, we designed and simulated a InAs QD embedded GaAs solar cell in SILVACO. With the insertion of quantum dot the efficiency of GaAs cell improved. The proposed cell thickness is  $4.67\mu\text{m}$  with 15 QD layers. From the simulation results it found that the proposed cell has efficiency of 36.97% where  $J_{sc} = 32.90$ ,  $V_{oc}=1.25$  and  $FF = 89.9\%$ . The quantum dots inserted are indeed helpful for solar cells to absorb lower energy photons which have longer wavelength from 875nm to 1200nm. Therefore, if we insert more QD layer with different size of QDs in the intrinsic layer the efficiency will be improve but side by side cost will be increased.

## Chapter 5

### Reference

1. <http://whatis.techtarget.com/definition/solar-power>
2. <http://whatis.techtarget.com/definition/photovoltaic-cell-PV-Cell>
3. <https://www.reference.com/science/solar-energy-important-323345a2f5340b84>
4. [http://www.mpoweruk.com/solar\\_power.htm](http://www.mpoweruk.com/solar_power.htm)
5. <http://energyinformative.org/best-solar-panel-monocrystalline-polycrystalline-thin-film/>
6. [https://en.wikipedia.org/wiki/Thin-film\\_solar\\_cell](https://en.wikipedia.org/wiki/Thin-film_solar_cell)
7. [https://en.wikipedia.org/wiki/Organic\\_solar\\_cell](https://en.wikipedia.org/wiki/Organic_solar_cell)
8. <http://optics.org/news/4/1/36>
9. [https://en.wikipedia.org/wiki/Third-generation\\_photovoltaic\\_cell](https://en.wikipedia.org/wiki/Third-generation_photovoltaic_cell)
10. <http://qtech-group.com/QTG/history/>
11. <http://www.azonano.com/article.aspx?ArticleID=1376>
12. <https://www.intechopen.com/books/solar-cells-new-approaches-and-reviews/quantum-dots-solar-cells>
13. <https://www.intechopen.com/books/solar-cells-new-approaches-and-reviews/quantum-dots-solar-cells>
14. <https://www.nrel.gov/pv/>
15. ALuque, AMarti, ANozik, "Solar cells based on quantum dots," MRS bulletin, 2007, 32:236-241